

# Synthesis and Characterization of Three-Dimensionally Ordered Macroporous Carbon/Titania Nanoparticle Composites

Zhiyong Wang, Nicholas S. Ergang, Mohammed A. Al-Daous, and Andreas Stein\*

Department of Chemistry, University of Minnesota, 207 Pleasant St. S.E., Minneapolis, Minnesota 55455

Received August 18, 2005. Revised Manuscript Received October 27, 2005

Three-dimensionally ordered macroporous (3DOM) carbon/titania nanoparticle composites were prepared in a program aimed at developing methods for assembling integrated multifunctional porous materials. The host material, 3DOM carbon, was synthesized by colloidal crystal templating with poly(methyl methacrylate) spheres, using a resorcinol–formaldehyde sol as a carbon source. This 3DOM support was pretreated with nitric acid to enhance the surface charge, and surface functional groups were characterized by Fourier transform infrared spectroscopy and acid–base titration. The modified support was then precoated with multiple layers of polyelectrolytes and finally coated with TiO<sub>2</sub> nanoparticles using the hydrothermal reaction of an aqueous solution of titanium(IV) bis(ammonium lactato) dihydroxide (TAL) at varying concentrations, temperatures, and reaction times. Higher hydrothermal reaction temperatures favored the formation of larger TiO<sub>2</sub> crystallites. The coating thickness increased at higher titanium precursor concentrations. Powder X-ray diffraction patterns indicated that the phase composition of the TiO<sub>2</sub> layer varied with different synthesis conditions. Scanning electron microscopy images revealed that the most uniform coating of TiO<sub>2</sub> was obtained at a reaction temperature of 200 °C with a TAL concentration of 0.2 M. This sample was characterized in more detail, using transmission electron microscopy, thermogravimetric analysis, differential scanning calorimetry, and nitrogen-sorption techniques.

## Introduction

Macroporous materials have been widely studied recently, because of their potential applications as photonic crystals,<sup>1–4</sup> filtration and separation agents,<sup>5,6</sup> anode materials in Li-ion batteries,<sup>7,8</sup> and catalyst supports.<sup>9</sup> Three-dimensionally ordered macroporous (3DOM) materials (also called “inverse opals” or “inverted opals”) are those prepared by utilizing face-centered cubic colloidal crystals that are composed of monodisperse silica, poly(methyl methacrylate) (PMMA), or polystyrene (PS) spheres as templates.<sup>10</sup> Recently, many 3DOM materials have been reported, including metals and alloys, metal oxides, polymers, SiC, bioactive glasses, nitrides, and phosphides.<sup>4,11–15</sup> 3DOM titania materials have

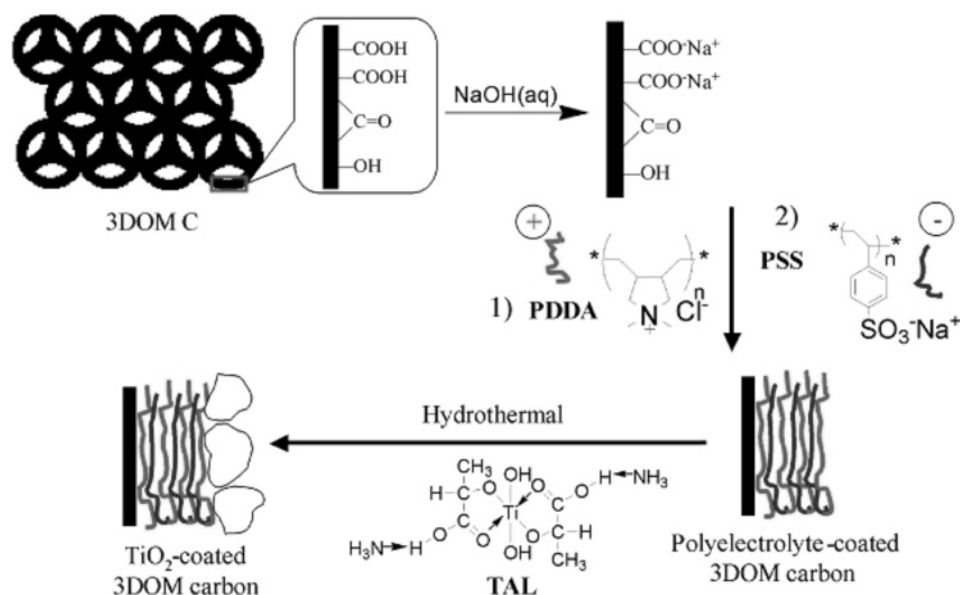
been fabricated, mainly as photonic crystals, using different colloidal templates and precursors.<sup>16–21</sup>

Among these materials, 3DOM carbon is particularly interesting, because it can readily be prepared in monolithic form, it is a good sorbent for organic molecules, and it is electrically conductive, which makes it possible to be used as an electrode for lithium batteries, super-capacitors or sensors.<sup>8,22,23</sup> In this study, 3DOM carbon is synthesized from a resorcinol–formaldehyde (RF) sol–gel carbon precursor, using PMMA colloidal crystals as templates, followed by the decomposition of PMMA and the pyrolysis (carbonization) of the carbon precursor. Pekala et al. first reported the

\* To whom correspondence should be addressed. Tel.: (612) 624-1802. Fax: (612) 626-7541. E-mail: stein@chem.umn.edu.

- (1) Lodahl, P.; van Driel, A. F.; Nikolaev, I. S.; Iman, A.; Overgaag, K.; Vanmaekelbergh, D.; Vos, W. L. *Nature* **2004**, *430*, 654–657.
- (2) Blanco, A.; Chomski, E.; Grabtchak, S.; Ibisate, M.; John, S.; Leonardo, S. W.; Lopez, C.; Meseguer, F.; Miguez, H.; Mondia, J. P.; Ozin, G. A.; Toader, O.; Van Driel, H. M. *Nature* **2000**, *405*, 437–440.
- (3) Tetreault, N.; Miguez, H.; Ozin, G. A. *Adv. Mater.* **2004**, *16*, 1471–1476.
- (4) Norris, D. J.; Vlasov, Y. A. *Adv. Mater.* **2001**, *13*, 371–376 and references therein.
- (5) Nakanishi, K. M.; Soga, N.; Tanaka, N. *J. Sol–Gel Sci. Technol.* **1998**, *13*, 163–169.
- (6) Sarrade, S. J.; Rios, G. M.; Carles, M. *Sep. Purif. Technol.* **1998**, *14*, 19–25.
- (7) Sakamoto, J.; Dunn, B. J. *Mater. Chem.* **2002**, *12*, 2859–2861.
- (8) Lee, K. T.; Lytle, J. C.; Ergang, N. S.; Oh, S. M.; Stein, A. *Adv. Funct. Mater.* **2005**, *15*, 547–556.
- (9) Diddams, P. In *Inorganic Supports and Catalysts*; Smith, K., Ed.; Ellis Horwood: New York, 1992; pp 3–39.
- (10) Schrodén, R. C.; Stein, A. In *Colloids and Colloid Assemblies: Synthesis, Modification, Organization and Utilization of Colloid Particles*; Caruso, F., Ed.; Wiley–VCH: Weinheim, Germany, 2004; pp 464–493 and references therein.

- (11) Kulinowski, K. M.; Jiang, P.; Vaswani, H.; Colvin, V. L. *Adv. Mater.* **2000**, *12*, 833–838 and references therein.
- (12) *Adv. Mater.* **2001**, *13*, 369–450. (Special Issue on Photonic Crystals.)
- (13) Xia, Y.; Gates, B.; Li, Z. Y. *Adv. Mater.* **2001**, *13*, 409–413 and references therein.
- (14) Velev, O. D.; Lenhoff, A. M. *Curr. Opin. Colloid Interface Sci.* **2000**, *5*, 56–63 and references therein.
- (15) Stein, A.; Schrodén, R. C. Designing Porous Solids Over Multiple Pore Size Regimes. In *Nanostructure Science and Technology*; Jones, C. W., Scott, S. L., Crudden, C. M., Eds.; Kluwer Plenum: Dordrecht, The Netherlands, 2002; Vol. 3, pp 257–276 and references therein.
- (16) Johnson, N. P.; McComb, D. W.; Richel, A.; Treble, B. M.; De La Rue, R. M. *Synth. Met.* **2001**, *116*, 469–473.
- (17) Dong, W.; Bongard, H. J.; Marlow, F. *Chem. Mater.* **2003**, *15*, 568–574.
- (18) Ni, P.; Cheng, B.; Zhang, D. *Appl. Phys. Lett.* **2002**, *80*, 1879–1881.
- (19) Schrodén, R. C.; Al-Daous, M.; Blanford, C. F.; Stein, A. *Chem. Mater.* **2002**, *14*, 3305–3315.
- (20) Kuai, S.; Badilescu, S.; Bader, G.; Bruning, R.; Hu, X.; Truong, V.-V. *Adv. Mater.* **2003**, *15*, 73–75.
- (21) Subramanian, G.; Manoharan, V. N.; Thorne, J. D.; Pine, D. J. *Adv. Mater.* **1999**, *11*, 1261–1265.
- (22) Zakhidov, A. A.; Baughman, R. H.; Iqbal, Z.; Cui, C.; Khayrullin, I.; Dantas, S. O.; Marti, J.; Ralchenko, V. G. *Science* **1998**, *282*, 897–901.
- (23) Zhou, Z.; Yan, Q.; Su, F.; Zhao, X. S. *J. Mater. Chem.* **2005**, *15*, 2569–2574.

Scheme 1. Coating of TiO<sub>2</sub> onto 3DOM Carbon<sup>a</sup>

<sup>a</sup> Detailed steps: First, 3DOM carbon is treated with concentrated HNO<sub>3</sub>, to introduce carboxylic acid groups. After washing with NaOH(aq), these groups are converted to negatively charged carboxylate groups. The carbon surface is then precoated alternately with PDPA (positively charged) and PSS (negatively charged) in the sequence of PDPA/PSS/PDPA/PSS/PDPA/PSS/PDPA. Finally, this polyelectrolyte-coated material is infiltrated with TAL solution and hydrothermally reacted to form a TiO<sub>2</sub> coating on the pore wall surface of 3DOM carbon.

synthesis of RF-based organic sol-gels through hydrolysis–condensation reaction mechanisms.<sup>24</sup> The combination of this synthesis with colloidal crystal templating produces macroporous carbon xerogels, whose pores are large enough to permit modification with nanoparticles, such as titania nanoparticles.

Titania, which is a wide-band gap semiconductor with a high dielectric constant, high refractive index, and good resistance to chemical attack, is widely used in applications including pigments, solar cells, humidity and gas sensors, photocatalytic degradation, selective reduction of NO<sub>x</sub>, purification, odor control, and sterilization.<sup>25–29</sup> Coatings of TiO<sub>2</sub> thin layers onto carbon nanotubes have been prepared with the hope of enhancing the photocatalytic performance<sup>30,31</sup> or for potential applications as sensors, nano-switches, and other devices.<sup>32</sup> Recently, TiO<sub>2</sub> nanoparticles have been coated onto glassy carbon, activated carbon, and graphite for the modification of carbon electrodes and photocatalytic applications.<sup>33–35</sup> Titania coatings have been shown to enhance the oxidation resistance of carbon fibers.<sup>36</sup> In this study, 3DOM carbon is used as a host for TiO<sub>2</sub> nanoparticles, because the open 3DOM architecture can

provide a highly accessible large support surface and the resulting composite materials can combine the properties of macroporous carbon and titania particles for applications including sensing, photocatalysis, and sorption.

The steps of the coating process are described schematically in Scheme 1. For the hydrothermal growth of titania on the surface of 3DOM carbon, titanium(IV) bis(ammonium lactato) dihydroxyde (TAL) is a particularly useful precursor, because it can be used in aqueous form and can produce relatively small nanoparticles in a hydrothermal reaction.<sup>37</sup> Before coating, extensive surface preparation is required. First, the surface of 3DOM carbon is oxidized using concentrated nitric acid to introduce carboxylic acid groups.<sup>38</sup> Nitric acid-treated 3DOM carbon is then neutralized with NaOH(aq) to produce a negatively charged, carboxylate-functionalized surface, which can be coated with alternating layers of poly(diallyldimethylammonium chloride) (PDPA, positively charged) and poly(4-styrenesulfonate sodium) salt (PSS, negatively charged), with PDPA as the outermost layer to facilitate coating with a negatively charged TiO<sub>2</sub> layer.<sup>39</sup> The aim of coating the carbon surface with multilayer polyelectrolytes via layer-by-layer (LbL) growth<sup>39,40</sup> is to increase the TiO<sub>2</sub> coating uniformity. Indeed, based on information from scanning electron microscopy (SEM) images, uniform titania coatings could be obtained using this procedure. However, the exact nature of the coating was dependent on several synthesis parameters, including the concentration of the TAL precursor and the temperature and duration of the hydrothermal synthesis.

- (24) Pekala, R. W. *J. Mater. Sci.* **1989**, *24*, 3221–3227.  
 (25) Bach, U.; Tachibana, Y.; Moser, J.-E.; Haque, S. A.; Durrant, J. R.; Graetzel, M.; Klug, D. R. *J. Am. Chem. Soc.* **1999**, *121*, 7445–7446.  
 (26) Tang, H.; Prasad, K.; Sanjines, R.; Levy, F. *Sens. Actuators B* **1995**, *26–27*, 71–75.  
 (27) Stafford, U.; Gray, K. A.; Kamat, P. V. *J. Phys. Chem.* **1994**, *98*, 6343–6351.  
 (28) Ciambelli, P.; Bagnasco, G.; Lisi, L. *Appl. Catal., B* **1992**, *1*, 61–77.  
 (29) Fujishima, A.; Rao, T. N.; Tryk, D. A. *J. Photochem. Photobiol. C: Photochem. Rev.* **2000**, *1*, 1–21.  
 (30) Lee, S.; Sigmund, W. M. *Chem. Commun.* **2003**, 780–781.  
 (31) Kedem, S.; Schmidt, J.; Paz, Y.; Cohen, Y. *Langmuir* **2005**, *21*, 5600–5604.  
 (32) Sainsbury, T.; Fitzmaurice, D. *Chem. Mater.* **2004**, *16*, 3780–3790.  
 (33) Yuan, S.; Hu, S. *Electrochim. Acta* **2004**, *49*, 4287–4293.  
 (34) Zhang, Y.; He, P.; Hu, N. *Electrochim. Acta* **2004**, *49*, 1981–1988.  
 (35) Lee, D.-K.; Kim, S.-C.; Kim, S.-J.; Chung, I.-S.; Kim, S.-W. *Chem. Eng. J.* **2004**, *102*, 93–98.

- (36) Xiao, Y.; Che, J.; Ji, F. *Mater. Chem. Phys.* **2004**, *83*, 104–106.  
 (37) Mockel, H.; Giersig, M.; Willig, F. *J. Mater. Chem.* **1999**, *9*, 3051–3056.  
 (38) Saliger, R.; Fischer, U.; Herta, C.; Fricke, J. *J. Non-Cryst. Solids* **1998**, *225*, 81–85.  
 (39) Decher, G. *Science* **1997**, *277*, 1232–1237 and references therein.  
 (40) Caruso, F. *Adv. Mater.* **2001**, *13*, 11–22 and references therein.

## Experimental Section

**Materials.** Chemicals used in this experiment were obtained from the following sources: 2,2'-azobis(2-methyl propionamide) dihydrochloride (AMPD) initiator (97%), methyl methacrylate monomer (MMA) (99%), resorcinol (99+%), hydrochloric acid volumetric standard (0.1 N solution in water), Bromocresol green/Methyl red mixed indicator (solution in methanol), poly(diallyldimethylammonium chloride) polyelectrolyte (PDDA) (20 wt % in H<sub>2</sub>O, molecular weight of  $M_w = 200\,000\text{--}350\,000$ ), poly(4-styrenesulfonate sodium) salt (PSS; powder,  $M_w \approx 700\,000$ ), and titanium(IV) bis(ammonium lactato) dihydroxide (TAL, 50 wt % in H<sub>2</sub>O) were all purchased from Aldrich; formaldehyde (37% in H<sub>2</sub>O) was from Fisher Scientific; sodium carbonate catalyst (anhydrous, 99.7%) was obtained from J.T. Baker; concentrated nitric acid (HNO<sub>3</sub>; 69.6% in H<sub>2</sub>O) and sodium hydroxide (NaOH; pellets, 99%) were purchased from Mallinckrodt. All chemicals were used as received. Deionized (DI) water used in all syntheses was purified to a resistivity greater than 18 M $\Omega$  cm. Stainless steel autoclaves (23 mL) with Teflon liners were obtained from the Parr Instrument Company.

**Preparation of 3DOM Carbon.** 3DOM carbon supports were synthesized from colloidal crystals of monodisperse PMMA spheres. PMMA spheres were prepared by emulsifier-free emulsion polymerization of MMA at 70 °C with AMPD as an initiator, as described elsewhere.<sup>41</sup> The resulting PMMA sphere suspension was transferred to a glass crystallization dish and stored for several weeks at room temperature without agitation. After the evaporation of water, PMMA spheres deposited on the bottom of the container, forming opalescent colloidal crystal pieces. 3DOM carbon was prepared according to a modified recipe reported elsewhere.<sup>8</sup> Approximately 10 pieces of PMMA with typical dimensions of ca. 1 cm  $\times$  1.5 cm  $\times$  0.2 cm were transferred to a 250-mL filtration flask, which was covered with a rubber septum and then placed under vacuum for ca. 1 h. 15 g resorcinol (R), 20 mL formaldehyde (F), and 0.24 g Na<sub>2</sub>CO<sub>3</sub> (C) were mixed and vigorously stirred for  $\sim$ 15 min at room temperature (RT) to form a homogeneous yellow solution (R:F:C molar ratio of 60:120:1). This solution was immediately injected into the flask, using a syringe, and PMMA pieces were infiltrated for ca. 2 h under vacuum. Subsequently, the PMMA/RF composites were transferred to a covered container and cured at 80 °C for 3 days, followed by continued curing without a cover at the same temperature overnight. Covering during the early stage prevented a loss of RF monomers or oligomers from the reaction system, while uncovering during the later stage facilitated the evaporation of moisture from the composite. Finally, the composites were heated under flowing nitrogen in a ceramic combustion boat inside a quartz tube at 900 °C for 2 h with heating and cooling rates of 5 °C/min. All the resulting carbon films were polished with sand paper before further use, to remove any nontemplated crust.

**Preparation of 3DOM Carbon with TiO<sub>2</sub> Coating.** 3DOM carbon pieces were submersed in concentrated nitric acid at 130 °C for 1 h, followed by multiple washings with DI water. 3DOM carbon samples were then dried in a vacuum desiccator at RT, neutralized with 0.1 M NaOH(aq), and washed with DI water. Alternate coatings of polyelectrolytes were prepared using the following sequence: PDDA/PSS/PDDA/PSS/PDDA/PSS/PDDA. The concentrations of the aqueous polyelectrolyte (PDDA and PSS) solutions were 5 mg/mL with additional 0.1 M NaCl. Before each coating step, carbon films were dried and evacuated before the

polyelectrolyte solutions were injected. After each coating step, carbon films were washed with DI water to remove residues. The 3DOM carbon films were then infiltrated with TAL(aq) solutions and hydrothermally reacted under different conditions. Three series of experiments were performed to study the coating results:

- (1) Different TAL concentrations: 0.01, 0.1, and 0.2 M at 200 °C for 24 h;
- (2) Different reaction durations: 0.05 M TAL(aq), reacted at 200 °C for 24, 48, and 72 h; and
- (3) Different reaction temperatures: 0.2 M TAL(aq) reacted at 140, 190, and 240 °C for 24 h.

After reaction, the products were washed and sonicated in DI water several times before analysis.

**Characterization.** Powder X-ray diffraction (XRD) patterns were acquired using a Bruker AXS microdiffractometer with a 2.2 kW sealed Cu X-ray source and a Hi-Star 2-D area detector. The generator voltage was 45 kV, and the current was 40 mA. Before measurement, small amounts of the powder samples were attached onto the top of a piece of flat quartz, which was attached to an aluminum stub. Fourier transform infrared (FT-IR) spectra in the mid-IR range (4000–400 cm<sup>-1</sup>) were obtained on a Nicolet Magna-IR 760 spectrometer using potassium bromide (KBr) pellets of the samples in a nitrogen atmosphere. C, H, O, and N elemental analyses (EA) of 3DOM carbon were performed by Atlantic Microlab, Inc. (Norcross, GA). Morphological information was obtained using a JEOL model 6700 SEM microscope with an accelerating voltage of 1.5 kV. Samples were mounted on conductive carbon tabs supported by an aluminum stub and were then coated with 50-Å-thick platinum thin films. Transmission electron microscopy (TEM) was conducted on a JEOL model JEM-1210 electron microscope that was operated at 120 kV. Samples for TEM measurements were drop-dried from ethanol onto a holey carbon film supported on a copper grid. Thermogravimetric analysis (TGA) and differential scanning calorimetry (DSC) were performed on a Netzsch model STA 409 instrument to determine the TiO<sub>2</sub>-coating content. The sample was heated in an alumina crucible under airflow to 1000 °C at a rate of 10 °C/min. Nitrogen-sorption measurements were performed on a Micromeritics ASAP 2000 gas sorptometer. Samples were degassed to 0.003 mmHg for 20 h at 120–150 °C. Specific surface areas were calculated by the Brunauer–Emmett–Teller (BET) method, and pore sizes and volumes were estimated from pore size distribution curves from the adsorption branches of the isotherms.

Acid–base titration was used to determine the concentration of surface functional groups on 3DOM carbon quantitatively before and after oxidation by concentrated HNO<sub>3</sub> according to the method reported by Boehm et al.<sup>42</sup> In this experiment, four standard base solutions—NaOC<sub>2</sub>H<sub>5</sub> (solution in ethanol), NaOH(aq), Na<sub>2</sub>CO<sub>3</sub>(aq), and NaHCO<sub>3</sub>(aq)—were mixed, respectively, with ca. 25 mg finely ground 3DOM carbon powder and stirred for 48 h at RT. All base solutions were ca. 0.05 M; the exact concentrations of these solutions were determined by titration with standard HCl aqueous solution. The carbon particles were separated from solution by filtration using a 0.2  $\mu$ m PTFE syringe filter. The clear solutions were then titrated with 0.05 M HCl (aq) standard solution to determine unreacted bases. A Bromocresol green/Methyl red solution was used as an indicator for titration.

## Results and Discussion

**Characterization of the 3DOM Carbon Support.** As-synthesized 3DOM carbon samples were characterized by

(41) Schroden, R. C.; Al-Daous, M.; Sokolov, S.; Melde, B. J.; Lytle, J. C.; Stein, A.; Carbajo, M. C.; Fernandez, J. T.; Rodriguez, E. E. *J. Mater. Chem.* **2002**, *12*, 3261–3327.

(42) Boehm, H. P.; Diehl, E.; Heck, W.; Sappok, R. *Angew. Chem., Int. Ed.* **1964**, *76*, 742–751.



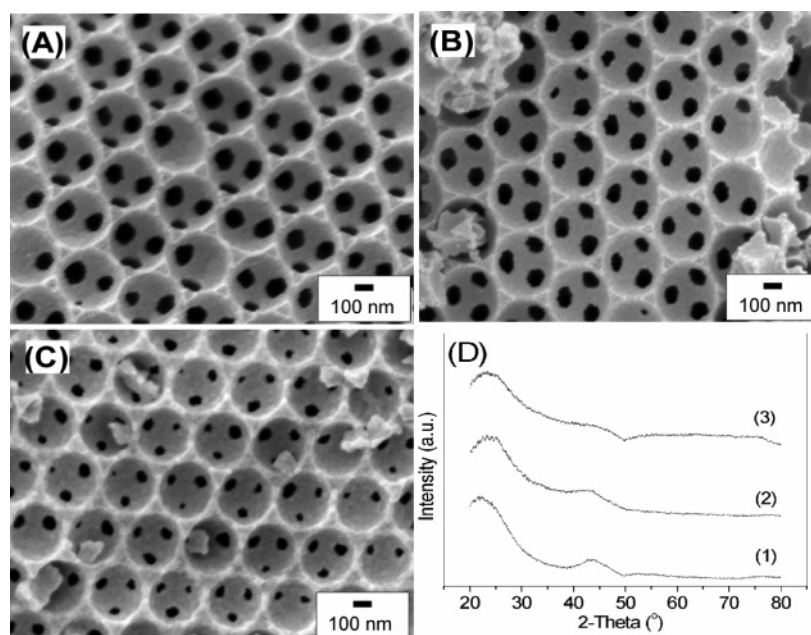


**Figure 1.** Scanning electron microscopy (SEM) images of (A) unmodified 3DOM carbon, (B) HNO<sub>3</sub>-treated 3DOM carbon, and (C) polyelectrolyte (PDDA/PSS/PDDA/PSS/PDDA/PSS/PDDA)-coated 3DOM carbon. Some voids contain fragments of 3DOM carbon produced during sample grinding for SEM analysis. Panel D shows powder XRD patterns, labeled (1), (2), and (3), corresponding to the samples shown in SEM images A, B, and C, respectively.

SEM, XRD, Fourier transform infrared (FT-IR) spectroscopy, and acid–base titration. 3DOM carbon exhibited a three-dimensionally ordered macroporous structure, as shown in the SEM image shown in Figure 1A. The XRD pattern of this sample (Figure 1D) revealed two broad reflection peaks. The first peak, at 22.9° 2 $\theta$  (0.39 nm), was assigned to the (002) reflection of graphene layers. This  $d$ -spacing was much larger than the interlayer spacing of 0.335 nm for graphite, as is typical for glassy carbon that is only partially ordered on the atomic scale.<sup>43</sup> The second peak, at 43.7° 2 $\theta$  (0.21 nm), arose from the (100) reflection of C atoms within graphene layers. After oxidation with HNO<sub>3</sub>, the 3DOM structure was maintained. However, the two characteristic diffraction peaks for graphene layers in 3DOM carbon<sup>8</sup> became broader and decreased in intensity after treatment. This was possibly due to bond breaking during oxidation, which led to greater disorder among graphene layers.

An FT-IR spectrum of the acid-treated sample (Figure 2) showed a sharp peak at 1730 cm<sup>-1</sup>, which was not observed for the unmodified 3DOM carbon. This absorption could be assigned to the  $\nu_{C=O}$  stretching vibration of carbonyl (–CHO) or carboxylic acid (–COOH) groups.<sup>44</sup> Broad peaks at 3425 cm<sup>-1</sup> and between 3000 and 2500 cm<sup>-1</sup> arose from the  $\nu_{O-H}$  stretching vibrations involving hydrogen bonding interactions between carboxyl, hydroxylactone, or phenol groups and adsorbed water. The overall intensity of these bands increased significantly after surface oxidation. Two other peaks remained mostly unchanged after acid treatment: one was located at 1580 cm<sup>-1</sup>, which has been assigned to the stretching of C=C bonds of the aromatic structure that are polarized by electronegative O atoms bound near one end

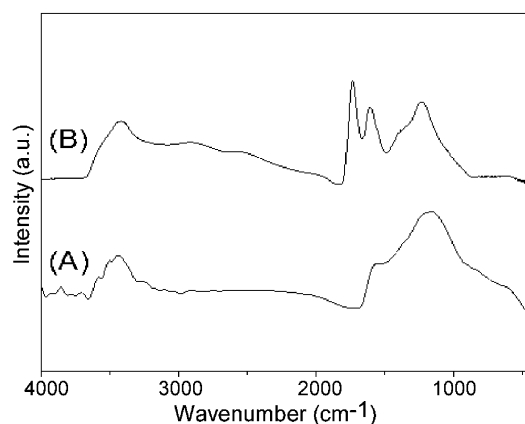


**Figure 2.** Fourier transform infrared (FT-IR) spectra of (A) 3DOM carbon calcined at 900 °C for 2 h and (B) 3DOM carbon treated with concentrated nitric acid at 130 °C for 1 h.

and, thus, become infrared-active,<sup>32,45</sup> and another absorption at 1200 cm<sup>-1</sup>, which is related to a carbon skeletal vibration.<sup>46</sup> Considering the structure of RF carbon, this peak may result from stretching vibrations of C–O bonds, such as C–OH in carboxyl groups, phenols, alcohols, or ethers.<sup>8,45</sup> The existence of epoxide groups is another possibility.<sup>47</sup>

Acid–base titration was used to quantify several possible surface functional groups on the carbon surface: ketone, phenol, lactone, lactol, carboxylic acid, and carboxylic anhydride. Lactone, lactol, carboxylic acid, and anhydride groups are of interest in this experiment, because they can be easily transformed to negatively charged carboxylate groups, which are indispensable to build polyelectrolyte multilayers, according to the route in Scheme 1. Local

(43) Oberlin, A.; Bonnamy, S.; Lafdi, K. Structure and Texture of Carbon Fibers. In *Carbon Fibers*; Donnet, J.-B., Ed.; Marcel Dekker: New York, 1998; pp 85–159.

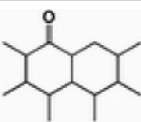
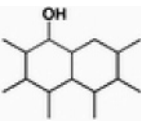
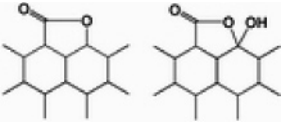
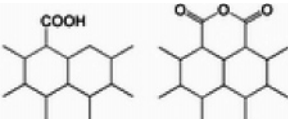
(44) Chen, J.; Hamon, M. A.; Hu, H.; Chen, Y.; Rao, A. M.; Eklund, P. C.; Haddon, R. C. *Science* **1998**, 282, 95–98.

(45) Boehm, H. P., Carbon Surface Chemistry. In *Graphite and Precursors*; Delhaes, P., Ed.; Gordon and Breach Science Publishers: Pessac, France, 2001; Vol. 7, p 141.

(46) Shaffer, M. S. P.; Fan, X.; Windle, A. H. *Carbon* **1998**, 36, 1603–1612.

(47) Meldrum, B. J.; Rochester, C. H. *J. Chem. Soc., Faraday Trans.* **1990**, 86, 2997.

Table 1. Titration Results for 3DOM Carbon before and after Oxidation with HNO<sub>3</sub>

name	local structure	Concentration (mmol/g) <sup>a</sup>	
		before oxidation	after oxidation
ketone		0.0293	2.07
phenol		0.0241	1.20
lactone and lactol		ND <sup>b</sup>	0.44
carboxylic acid and anhydride		ND <sup>b</sup>	3.26

<sup>a</sup> The units for the functional group concentrations are millimoles of functional groups per gram of carbon sample (expressed as mmol/g). <sup>b</sup> Not detected.

Table 2. Elemental Analyses of 3DOM Carbon before and after Oxidation with HNO<sub>3</sub>

sample element	3DOM Carbon		3DOM Carbon (HNO <sub>3</sub> )	
	weight percent (%)	mole ratio	weight percent (%)	mole ratio
C	93.29	1.000	67.85	1.000
H	0.61	0.078	1.41	0.248
O	4.06	0.033	27.69	0.306
N	0.32	0.003	0.56	0.007

structures for these functional groups and their concentrations calculated from titration data are displayed in Table 1.

Before HNO<sub>3</sub> treatment, only small amounts of ketone and phenol groups were present, which may originate from the RF organic gel. Lactone, lactol, and carboxyl groups were not detected by titration. After oxidation, the total surface functional group concentration increased ca. 130 times, with the largest concentration being observed for carboxyl groups. This was consistent with the FT-IR result, which showed a sharp and strong carbonyl peak.

Elemental analysis (Table 2) revealed that 3DOM carbon samples contained appreciable amounts of oxygen, both before (C<sub>1.00</sub>H<sub>0.078</sub>O<sub>0.033</sub>N<sub>0.003</sub>) and after nitric acid treatment (C<sub>1.00</sub>H<sub>0.248</sub>O<sub>0.306</sub>N<sub>0.007</sub>). A large fraction of the oxygen may have been due to the strong chemisorption of H<sub>2</sub>O (and possibly O<sub>2</sub> and CO<sub>2</sub>)<sup>45,48</sup> on the active surface of 3DOM carbon when the sample was exposed to air. After nitric acid treatment, the oxygen content increased drastically and hydrogen and nitrogen were also introduced. Possible sources for added oxygen include new oxygen-containing functional groups and additional adsorption of water due to increased surface polarity after oxidation. H originates from hydrogen-containing groups such as phenol and carboxyl. This is coincident with the titration results (see Table 1). The nitrogen content increased slightly, which may be due to the formation of the -NO<sub>2</sub> group during oxidation.<sup>49</sup>

From comparisons of titration (Table 1) and elemental analysis results (Table 2), we determined that the sample also contained nonacidic surface functional groups, which could not be detected by acid–base titration. The titratable oxygen content of the original 3DOM carbon was 0.085 wt % (ketone and phenol), i.e., much lower than the total oxygen content (4.06 wt %). This indicates that most O atoms in 3DOM carbon were nonacidic and relatively “inert” to the bases used in this titration. Considering the synthesis chemistry of resorcinol and formaldehyde, RF organic gels contain large fractions of -CH<sub>2</sub>OCH<sub>2</sub>- groups.<sup>50</sup> During the pyrolysis of the RF gel, these groups may decompose only partially. Therefore, the residue contributes to the high content of “inert” O atoms. Another reason for the lower titration results may have been the limited access of the basic reagents to very narrow micropores inside 3DOM carbon.

**Titania Coating on 3DOM Carbon.** Thin layers of crystalline TiO<sub>2</sub> were coated onto the 3DOM carbon pore walls under different hydrothermal reaction conditions. The results will be illustrated separately for varying precursor concentrations, reaction durations, and temperatures.

**1. Influence of TAL Concentration on Coatings.** Variations in the coating thickness with TAL concentration could be observed in the SEM images (see Figure 3A–C). As the TAL concentration was increased from 0.01 M to 0.2 M, the macropore wall thickness increased from ca. 50 nm to ca. 100 nm. Some of the windows between adjacent pores were infiltrated by TiO<sub>2</sub> nanoparticles, causing partial blockage of access. In Figure 3B, some randomly ordered, needlelike solids could be found at the external surface of the sample. These solids may be TiO<sub>2</sub> crystals formed inside macropores where the initial TAL content was higher before hydrothermal reaction. XRD patterns also provided information on the dependence of TiO<sub>2</sub> phases on Ti precursor concentration: when the solution was dilute (0.01 M), no

(48) Rouquerol, F.; Rouquerol, J.; Sing, K. *Adsorption by Powders and Porous Solids: Principles, Methodology, Applications*. Academic Press: New York, 1999.

(49) Salame, I. I.; Bandoz, T. J. *J. Colloid Interface Sci.* **2001**, *240*, 252–258.

(50) Al-Muhtaseb, S. A.; Ritter, J. A. *Adv. Mater.* **2003**, *15*, 101–114.

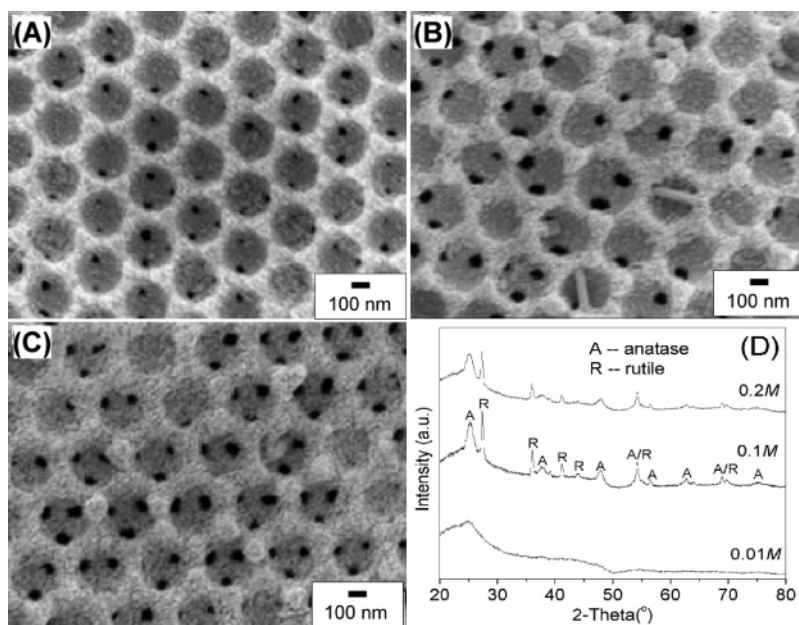


**Figure 3.** SEM images (panels A, B, and C) and powder XRD patterns (panel D) of TiO<sub>2</sub>-coated 3DOM carbon obtained by hydrothermal reaction at 200 °C, 24 h with the following TAL concentrations: (A) 0.01 M, (B) 0.1 M, and (C) 0.2 M.

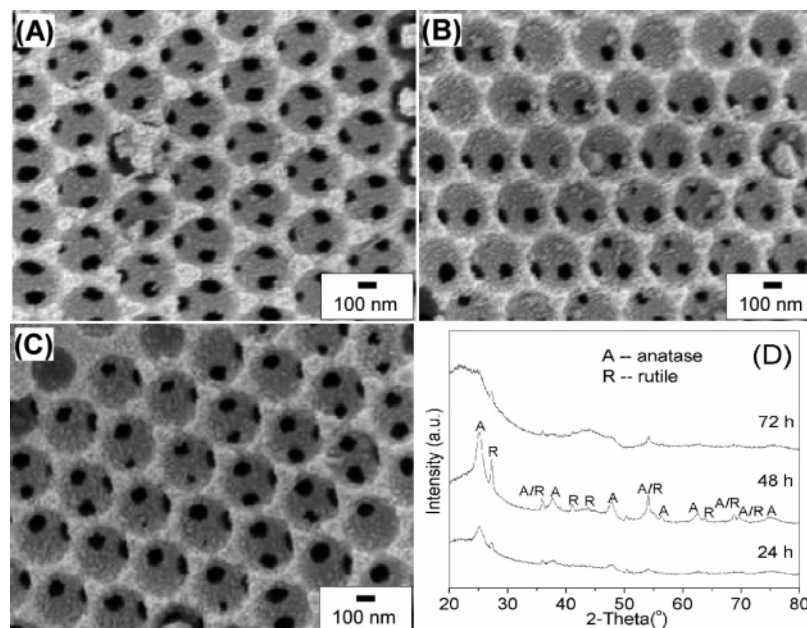


**Figure 4.** SEM images (panels A, B, and C) and powder XRD patterns (panel D) of TiO<sub>2</sub>-coated 3DOM carbon obtained hydrothermally with 0.05 M TAL(aq) at 200 °C for (A) 24 h, (B) 48 h, and (C) 72 h.

crystalline TiO<sub>2</sub> was detected and only a broad peak from amorphous carbon near 25° 2 $\theta$  could be observed. As the concentration was increased by a factor of 10 or higher (from 0.01 M to 0.1 M and 0.2 M), mixed phases of anatase and rutile were formed on the sample surface.

**2. Influence of Reaction Duration on Coatings.** SEM images (Figure 4 A, B, and C) showed the results of treating 3DOM carbon with 0.05 M TAL aqueous solutions at 200 °C for different times. No difference in the morphologies of the TiO<sub>2</sub> coatings was evident. Pore diameters and wall thicknesses did not vary significantly when the reaction time was increased. However, the identity of the titania phases was strongly related to the reaction time, as shown in the powder XRD patterns (Figure 4D). Based on observed intensity increases and line narrowing, the coating layers

became more crystalline and crystallite sizes increased with longer reaction times from 24 to 48 h. After an even longer reaction time (3 days), intensities of all the TiO<sub>2</sub> peaks decreased, compared to the background (broad amorphous carbon peaks).

**3. Influence of Reaction Temperature on Coatings.** The reaction temperature had a more significant influence on the morphology of titania coatings. This could be clearly observed in the SEM images (see Figure 5A, B, and C). At a low temperature (140 °C), fine TiO<sub>2</sub> particles on the pore wall surfaces were <100 nm. As the temperature was increased to 190 °C, some particles with sizes of ca. 100–200 nm could be seen on the 3DOM carbon pore walls (Figure 5B). At 240 °C, a great amount of TiO<sub>2</sub> particles >150 nm in size began to form freely on the external sample



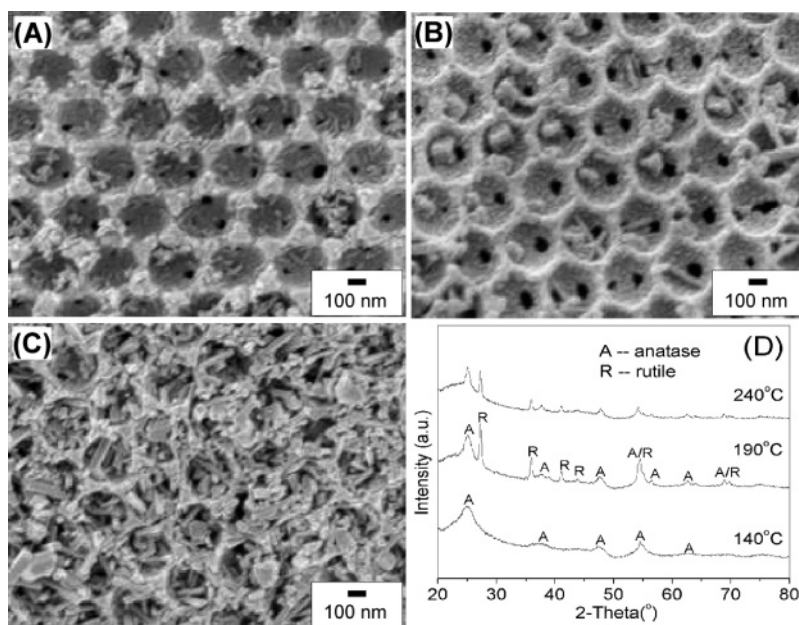


**Figure 5.** SEM images (panels A, B, and C) and powder XRD patterns (panel D) of  $\text{TiO}_2$ -coated 3DOM carbon obtained by hydrothermal reaction with 0.2 M TAL at temperatures of (A) 140 °C, (B) 190 °C, and (C) 240 °C for 24 h.

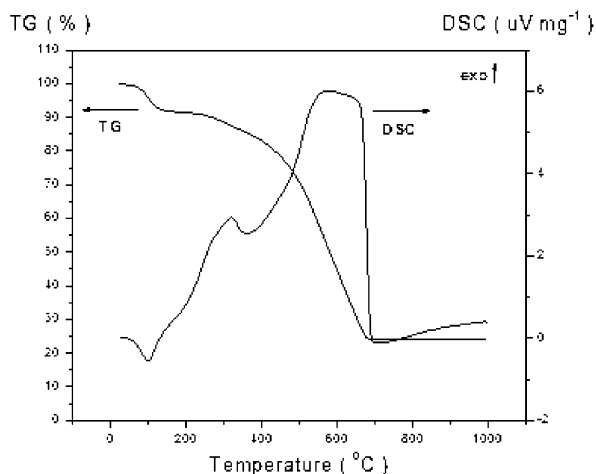


**Figure 6.** Thermogravimetric analysis (TGA) and differential thermal calorimetry (DSC) curve of  $\text{TiO}_2$ -coated 3DOM carbon hydrothermally reacted with 0.2 M TAL at 200 °C for 24 h. The analysis was performed in air.

surface and inside macropores, instead of on the pore walls. According to published thermal decomposition studies, PDDA begins to decompose at temperatures of  $>200$  °C, whereas PSS decomposes at a temperature of  $>550$  °C.<sup>51,52</sup> Therefore, the reason for the free growth of crystals in 3DOM carbon macropores at 240 °C may be that polyelectrolyte layers, especially PDDA, became detached from the 3DOM carbon pore wall, a process that inverted the surface charge from positive to negative. Therefore,  $\text{TiO}_2$  particles precipitated directly inside macropores from the TAL solution, because of the mismatch of surface charges between the 3DOM carbon pore walls and the  $\text{TiO}_2$  nanoparticles.

In addition to modifying the morphology, temperature affected the crystalline phase of the titania coating layers.

The transformation of  $\text{TiO}_2$  phases was confirmed by powder XRD. At a lower temperature (140 °C), only anatase was present. When the temperature was increased to 190 °C, rutile was detected. An increase to even higher temperature (240 °C) resulted in no significant change of the phase composition. XRD patterns also revealed that titania particles grew larger as the reaction temperature was increased, as judged from the narrowing of the anatase (101) reflection from 140 °C to 240 °C. This observation coincided with results reported by Mockel et al. for homogeneous synthesis conditions for titania nanoparticles in the aqueous phase.<sup>37</sup> However, in their work, only anatase was found in the products, while mixed phases of anatase and rutile were observed in our study, where titania was grown on the polyelectrolyte-modified carbon support. The reason may be the different environment for the formation of titania crystallites. In the homogeneous synthesis, titania nanoparticles precipitated directly from the TAL solution, where the initial nuclei of crystal seeds were only surrounded by an aqueous solution during formation. In the synthesis described here, the surface charge density on 3DOM carbon pore walls was much higher than that in the pore bulk, so that titania crystal seeds formed on the pore wall surface selectively, influenced by the polyelectrolyte coating.

**Structural Characterization of the Optimized Composite.** Based on SEM results, the sample that was obtained via the hydrothermal reaction of 3DOM carbon with 0.2 M TAL solution at 200 °C for 24 h showed the most uniform coating (see Figure 3C). Therefore, further characterization of this sample was performed to evaluate the coating content and the microstructures of the carbon macropore wall and the titania coating.

Figure 6 shows results from thermogravimetric analysis. The TG curve revealed mainly three weight-loss stages. The first event occurred in the region of 80–150 °C, with a weight loss of 8% and probably involved the desorption of physically adsorbed water,  $\text{CO}_2$ , and hydrocarbons on the

(51) Huang, P. C.; Reichert, K.-H. *Angew. Makromol. Chem.* **1989**, *165*, 1–7.

(52) Chen, X.; Randall, P. D.; Perruchot, C.; Watts, F. J.; Patten, E. T.; Werne, T.; Armes, P. S. *J. Colloid Interface Sci.* **2003**, *257*, 56–64.

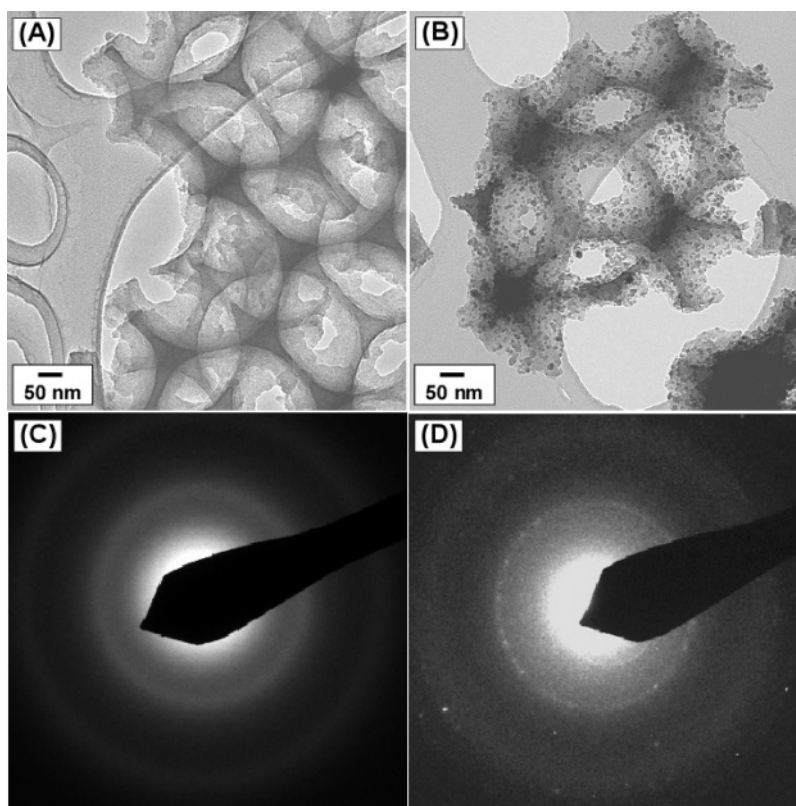


**Figure 7.** Transmission electron microscopy (TEM) images of 3DOM carbon (A) before coating and (B) after coating with  $\text{TiO}_2$ . Panels C and D are selected area diffraction (SAD) patterns of regions in panels A and B, respectively. Synthesis conditions were the same as those described in Figure 6.

carbon surface.<sup>53</sup> This was also confirmed by the appearance of an endothermic peak at  $\sim 150^\circ\text{C}$  on the differential scanning calorimetry (DSC) trace. The second and third events occurred between the temperature ranges of ca.  $250\text{--}400^\circ\text{C}$  and  $400\text{--}700^\circ\text{C}$ , respectively, leading to a total weight loss of 68%. DSC showed two exothermic peaks in these ranges: one at  $300^\circ\text{C}$  and another at  $600^\circ\text{C}$ . As discussed previously, the first peak at  $300^\circ\text{C}$  may be due to the burning of polyelectrolyte precoat layers. The second broad exotherm reflects the combustion of 3DOM carbon in the air atmosphere. After thermal analysis, a white powder was observed in the crucible, which contributed 24.0 wt % of the total sample mass. XRD showed that this powder was pure rutile-phase titania (see Figure S1 in the Supporting Information). This is consistent with studies that note that, at temperatures of  $>500^\circ\text{C}$ , other polymorphs transform to rutile.<sup>54</sup>

The coating was also characterized by transmission electron microscopy (TEM) (see Figure 7). Nanoparticles with diameters of ca. 10 nm on 3DOM carbon macropore walls could be clearly observed in the figure on the right-hand side, whereas, before coating, the walls were smooth. Moreover, before coating, the electron diffraction pattern showed only a series of halos for amorphous carbon (see Figure 7C). After coating, sharp diffraction rings and spots originating from anatase and rutile nanocrystals appeared (see Figure 7D).

Nitrogen-sorption measurements of untreated and surface-modified 3DOM carbon all showed a type-II isotherm with type-H4 hysteresis, which was most pronounced in the original 3DOM carbon (see Figure 8A). Type-II isotherms are characteristic of multilayer adsorption on surfaces of macroporous or nonporous materials, whereas type-H4 hysteresis loops result from slit-shaped pores, as are found in many activated carbons.<sup>8,48</sup> Pore size distribution curves indicated that all these samples had characteristic pores in the micropore range (see Figure 8B). However, the  $\text{TiO}_2$ -coated sample exhibited two small peaks, at 8 and 19 nm, which are in the range of the sizes of titania nanoparticles observed via TEM. Therefore, these peaks may reflect the porosity of those particle aggregates.

Results from  $\text{N}_2$ -adsorption analysis are summarized in Table 3. The original 3DOM carbon sample had a BET surface area of  $140\text{ m}^2/\text{g}$ . After oxidation with concentrated nitric acid, the surface area increased to  $431\text{ m}^2/\text{g}$ . During treatment in boiling  $\text{HNO}_3$ , some chemical bonds that link adjacent graphene layers, such as  $-\text{CH}_2-$  and  $-\text{CH}_2\text{OCH}_2-$ , and  $\text{C}=\text{C}$  bonds within graphene layers, could be destroyed, thus creating more defect sites and additional microporosity. This explanation was also supported by the observation that, after  $\text{HNO}_3$  treatment, the carbon monoliths became very brittle and by the XRD line broadening noted after oxidation (see Figure 1D). A significant decrease of surface area was observed for the polyelectrolyte-coated sample. The value of  $17\text{ m}^2/\text{g}$  corresponds approximately to the estimated surface area of the macropores. The large reduction in surface area suggests that almost all of the micropores and mesopores within the 3DOM carbon macropore walls were blocked by the polyelectrolytes. As a result, the contribution of micro-

(53) Fricke, J.; Petricevic, R. Carbon Aerogels. In *Handbook of Porous Solids*; Schuth, F.; Sing, K. S. W.; Weitkamp, J., Eds. Wiley-VCH: Weinheim, Germany, 2002; p 2037.

(54) Bokhimi, X.; Morales, A.; Aguilar, M.; Toledo-Antonio, J. A.; Pedraza, F. *Int. J. Hydrogen Energy* **2001**, 26, 1279–1287.



**Table 3. Brunauer–Emmett–Teller (BET) Surface Area, Micropore Area, and Average Pore Diameter of 3DOM Carbon, HNO<sub>3</sub>-Treated 3DOM Carbon, Polyelectrolyte-Coated 3DOM Carbon, and TiO<sub>2</sub>-Coated 3DOM Carbon**

sample	degassing temperature (°C)	BET surface area, $S_{\text{BET}}$ (m <sup>2</sup> /g)	micropore area (m <sup>2</sup> /g)	average pore diameter (nm)
3DOM C	150	140	108	2.1
3DOM C/HNO <sub>3</sub> <sup>a</sup>	120	431	353	1.7
3DOM C/PDDA-PSS <sup>a</sup>	120	17	5	6.5
3DOM C/TiO <sub>2</sub>	150	184	111	2.2

<sup>a</sup> These samples were degassed at a lower temperature to avoid decomposition of surface functional groups and polyelectrolytes. Note that the sorption data for 3DOM C/HNO<sub>3</sub> degassed at 200 °C were within 4% of the values shown for the sample degassed at 120 °C.

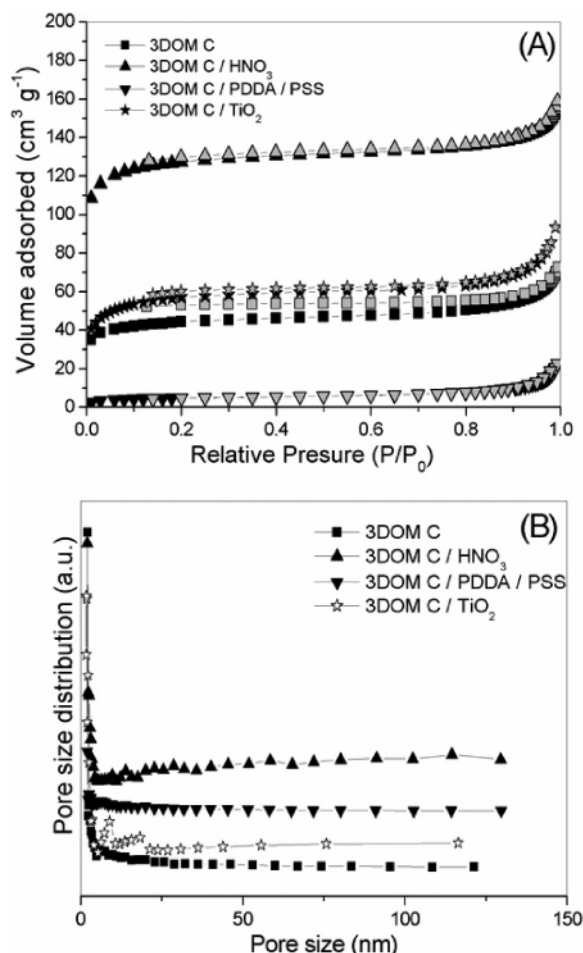


**Figure 8.** (A) Nitrogen-sorption isotherm and (B) adsorption-branch pore size distribution of 3DOM carbon, HNO<sub>3</sub>-treated 3DOM carbon, polyelectrolyte-coated 3DOM carbon, and TiO<sub>2</sub>-coated 3DOM carbon. Synthesis conditions for the TiO<sub>2</sub>-coated 3DOM carbon are the same as those described in Figure 6.

pores to the total surface area decreased from 77% (3DOM carbon) and 82% (HNO<sub>3</sub>-treated 3DOM carbon) to 29%, and the average pore diameter increased beyond micropore dimensions (6.5 nm). This was additional evidence for the successful coating with polyelectrolyte layers by the LbL method. After the growth of TiO<sub>2</sub> nanoparticles, the surface area increased again to 184 m<sup>2</sup>/g, the micropore contribution returned to 60.3%, and the average pore diameter decreased to 2.2 nm. These data indicated that the TiO<sub>2</sub> nanoparticle coatings contributed significantly to the overall porosity of the material, by creating textural micropores and mesopores.

### Conclusions

In this work, a new methodology of assembling integrated multifunctional porous materials, titania-coated three-

dimensionally ordered macroporous (3DOM) carbon was demonstrated. Surface functionalization was achieved within the confinement of macropores on three length scales: the molecular scale (introduction of surface functional groups on 3DOM carbon during oxidation), the macromolecular scale (layer-by-layer (LbL) coating of polyelectrolytes), and the nanoparticle scale (hydrothermal growth of nanocrystalline titania). The LbL technique of precoating the porous support with polyelectrolytes of alternating charges was used, mainly to build a uniform, positively charged surface layer within 3DOM carbon pores to facilitate hydrothermal growth of negatively charged titania nanoparticles. However, it had the additional effect of blocking micropores and reducing the BET surface area of the porous carbon by an order of magnitude. Thus, it can be used to modify the texture (microporosity and mesoporosity) of porous carbon materials. The sample with the most uniform titania coating was obtained when 3DOM carbon was reacted with 0.2 M titanium(IV) bis(ammonium lactate) dihydroxide (TAL) aqueous solution at 200 °C for 24 h. Thermogravimetric analysis (TGA) of this sample indicated that the TiO<sub>2</sub> coating contributed ~24% to the sample mass. Uniform TiO<sub>2</sub> nanoparticle coatings were observed clearly on electron microscopy images. Comparison of the N<sub>2</sub>-sorption isotherms for polyelectrolyte-coated and TiO<sub>2</sub>-coated 3DOM carbon samples revealed that the TiO<sub>2</sub> layer contributed textural microporosity and mesoporosity to the composite material. Powder X-ray diffractometry indicated that the crystal phase of the TiO<sub>2</sub> coatings was a mixture of anatase and rutile, but a pure anatase phase coating could be obtained at low temperature with a specific titanium precursor concentration. Higher hydrothermal reaction temperatures favored the formation of larger TiO<sub>2</sub> crystallites. The coating thickness increased at higher titanium precursor concentrations. In ongoing work, we are evaluating these novel composite materials as potential sensors, which combine the advantages of electrical conductivity and a high amount of accessible surface area.

**Acknowledgment.** This research was supported by the Office of Naval Research (under Grant No. N00014-01-1-0810, subcontracted from NWU), the Petroleum Research Foundation administered by the American Chemical Society (ACS-PRF Grant No. 42751-AC10) and in part by the MRSEC program of the NSF (DMR-0212302), which supports the University of Minnesota Characterization Facility.

**Supporting Information Available:** Powder XRD pattern of residue from TiO<sub>2</sub>-coated 3DOM carbon after TG measurement (PDF). This material is available free of charge via the Internet at <http://pubs.acs.org>.

CM051865K